STM JOURNALS

Journal of
Materials & Metallurgical Engineering

https://journals.stmjournals.com/jomme

ISSN: 2231-3818 (Online)
ISSN: 2321-4236 (Print)
Volume 15, Issue 1, 2025
January–April
DOI (Journal): 10.37591/JoMME

Research JoMME

Synthesis and Applications of Copper-Doped Pyridine Precipitate

P. Girija[1,2]*

Abstract

A metal organic nonlinear optical single crystal, copper doped pyridine material, was created at room temperature using the slow evaporation solution growth technique (SEST). The developed material's crystalline nature was revealed by a powder X-ray diffraction (XRD) analysis. Single crystal XRD study shows that the material synthesized possesses monoclinic system of cell parameters, a = 11.44 Å, b = 7.92 Å, C = 11.74 Å and alpha and gamma is equal to 90°, beta 110.40° differing from other two angles which shows that the synthesized material is new and not reported by any researchers before. Thermal studies of the sample material were also studied and confirmed that the synthesized material is temperature resistant revealing its application in laser technology. UV-visible-NIR spectroscopy confirms that the absorbance is in higher cutoff wavelength. The morphology and the presence of the metal copper is discussed in the scanning electron microscopy–energy dispersive X-ray spectroscopy ((SEM-EDS) specimen. Fourier transform infrared (FTIR) spectral studies confirm the synthesized material as copper-doped pyridine material. A novel copper-doped pyridine material was synthesized at room temperature using the slow evaporation solution growth technique (SEST). Powder and single-crystal XRD confirmed the monoclinic structure and uniqueness of the material. Thermal, UV-visible-NIR, SEM-EDS, and FTIR studies revealed its thermal resistance, optical properties, and chemical composition, making it suitable for laser technology applications. This green-colored material is reported for the first time.

Keywords: Pyridine, slow evaporation solution growth technique (SEST), copper sulfate, reflectance and energy dispersive spectroscopy

INTRODUCTION

Due to their technological significance in the domains of optical communication signal processing and instrumentation, nonlinear optical (NLO) materials exhibiting second harmonic generation have become increasingly sought after in recent decades [1–3]. Due to their significance in delivering essential activities such as frequency conversion, light modulation, and optical memory storage, semi-organic nonlinear optical materials are attracting attention from the current research trend [4, 5]. Inertial confinement fusion research is being facilitated by the wide range of applications for NLO single crystals, including electro-optic switching, optical memory storage, frequency conversion, second harmonic production, and high energy lasers [6, 7]. Although organic molecules have a high nonlinear coefficient of efficiency, they are prone to degradation and have low mechanical and thermal stability. The majority of organic materials have low laser damage thresholds, poor optical quality, and insufficient transparency [8]. Furthermore, organic materials cannot be used to fabricate devices since it is hard to generate big single crystals of them [9]. Due to the absence of broad π-

***Author for Correspondence**
P. Girija
E-mail: gk_au09@yahoo.com

[1]Assistant Professor, Department of Chemistry, Annamalai University, Chidambaram, Tamil Nadu, India
[2]Professor, Department of Chemistry, Arignar Anna Government Arts College (AAGAC), Villupuram, Tamil Nadu, India

Received Date: December 30, 2024
Accepted Date: January 19, 2025
Published Date: January 29, 2025

Citation: P. Girija. Synthesis and Applications of Copper-Doped Pyridine Precipitate. Journal of Materials & Metallurgical Engineering. 2025; 15(1): 51–60p.

electron delocalization, inorganic crystals have comparatively little optical nonlinearity despite having outstanding mechanical and thermal properties [7]. Semi-organic materials, on the other hand, have a combination of inorganic and organic properties. Semi-organic crystals, which are more suited for device manufacturing, are the subject of research due to their desirable properties [10]. The pyridine derivatives have already been shown to exhibit significant second harmonic nonlinearity [11]. There is a lot of fluorescence in the crystal environment around pyridines in their inorganic surroundings [12]. Copper plays an important role in many biochemical processes in the metabolism of all living cells, pyridine carboxylic acids as well as their derivatives also play an important role [13]. Pyridine-2,6-dicarboxamide is a chelating ligand for metal cation, small anions as well as small not charged molecules [14]. The potential use of pyridine-2,6-dicarboxamide synthetic derivatives in senescence-mediated anticancer therapy is demonstrated by their capacity to stabilize telomeric G-quadruplex DNA [15]. Electro-optic and spectroscopic studies of pyridine doped with boric acid salts and zinc salts have already been reported. Electron spin resonance (ESR) spectral studies of the pure and zinc-doped hexakis pyridine-N-oxile cuprate ion have been performed. A series of new crystal structure chlorometallic-pyridinium boric acid salts [16–18] were studied. Pyridine-doped copper salts have not been reported so far. In this paper, copper sulfate doped pyridine material was grown by slow evaporation solution growth method for the first time to yield a blue crystal and a green colored precipitate. Here we discuss only about the green colored precipitate and its characterization from the results of various studies like Fourier transform infrared (FTIR), single crystal X-ray diffraction (XRD(, powder XRD, UV-visible spectroscopy, thermogravimetry–differential thermal analysis (TG-DTA) and scanning electron microscopy–energy dispersive X-ray spectroscopy (SEM-EDS) of the green precipitate are reported.

MATERIALS AND METHODS

Synthesis and Crystal Growth

Pyridine is a basic heterocyclic compound known as azine having chemical formula C_5H_5N. Pyridine containing drugs are used as antimicrobial, antiviral, anticancer, antioxidant, antimalarial, antihypertensive, antidiabetic, antiamebic, psychopharmacological, antagonists and anti-inflammatory agents. Copper sulfate is an inorganic compound containing copper and sulfate, in its crystal form it is 'blue stone or blue vitriol' on the whole, copper sulfate acts as popular raw material for producing other type of copper compounds. The crystals of copper sulfate may be used as a fungicide, root killer, herbicide and algaecide in both agriculture and non-agriculture. Its primary uses are as a molluscicide and antibacterial. The synthesis now begins by forming a pyridine copper sulfate precipitate (material) at room temperature using an equimolar ratio (1:1) of pyridine (7 mL) and copper sulfate (25 g) in 100 mL of triply distilled water as a solvent. The mixed solutions of pyridine and copper sulfate were properly stirred for 3 to 5 hours in a conical flask using a magnetic stirrer and the contents in the conical flask is filtered to remove the formed precipitate. The filtered solutions were poured into beaker and covered with polythene sheet at the neck of beaker with holes on the top of covered sheet and kept for slow evaporation at ambient temperature and the formed green color precipitate is dried, packed and then labeled. Photographs of the grown pyridine copper sulfate crystals (formed from the filtrate) and formed green colored pyridine copper sulphate precipitate are shown in Figure 1.

RESULTS AND DISCUSSION

Thermal Studies

In order to know the thermal behavior of pyridine copper sulfate TG/DTA analysis was carried out in nitrogen atmosphere. The recorded TG/DTA curves are given in Figure 2.

A sharp endothermic peak obtained around 119, 219 and 295ºC shows the melting point of pyridine copper sulfate precipitate in DTA curve. There is no observed endothermic peak below this endothermic point, there is broad endothermic peaks at around 250ºC which may be due to liberation of water molecules.

Figure 1. Photographs of (a) blue pyridine copper sulfate crystal; (b) green pyridine copper sulfate precipitate.

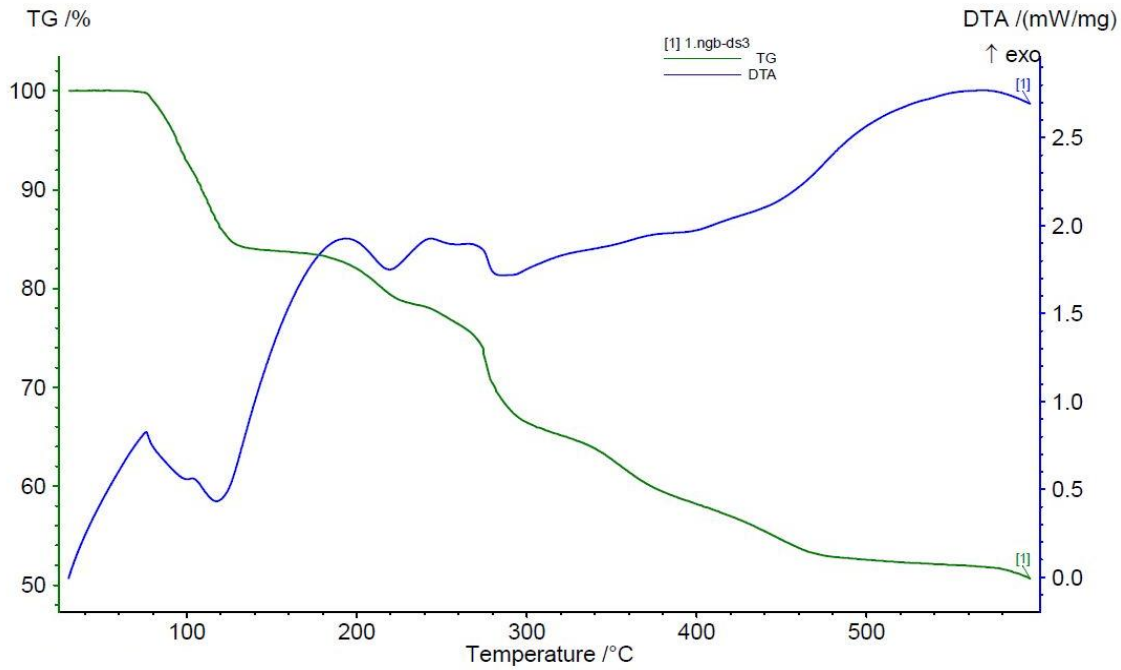

Figure 2. Thermogravimetry/differential thermal analysis (TG/DTA) curves of pyridine copper sulfate precipitate.

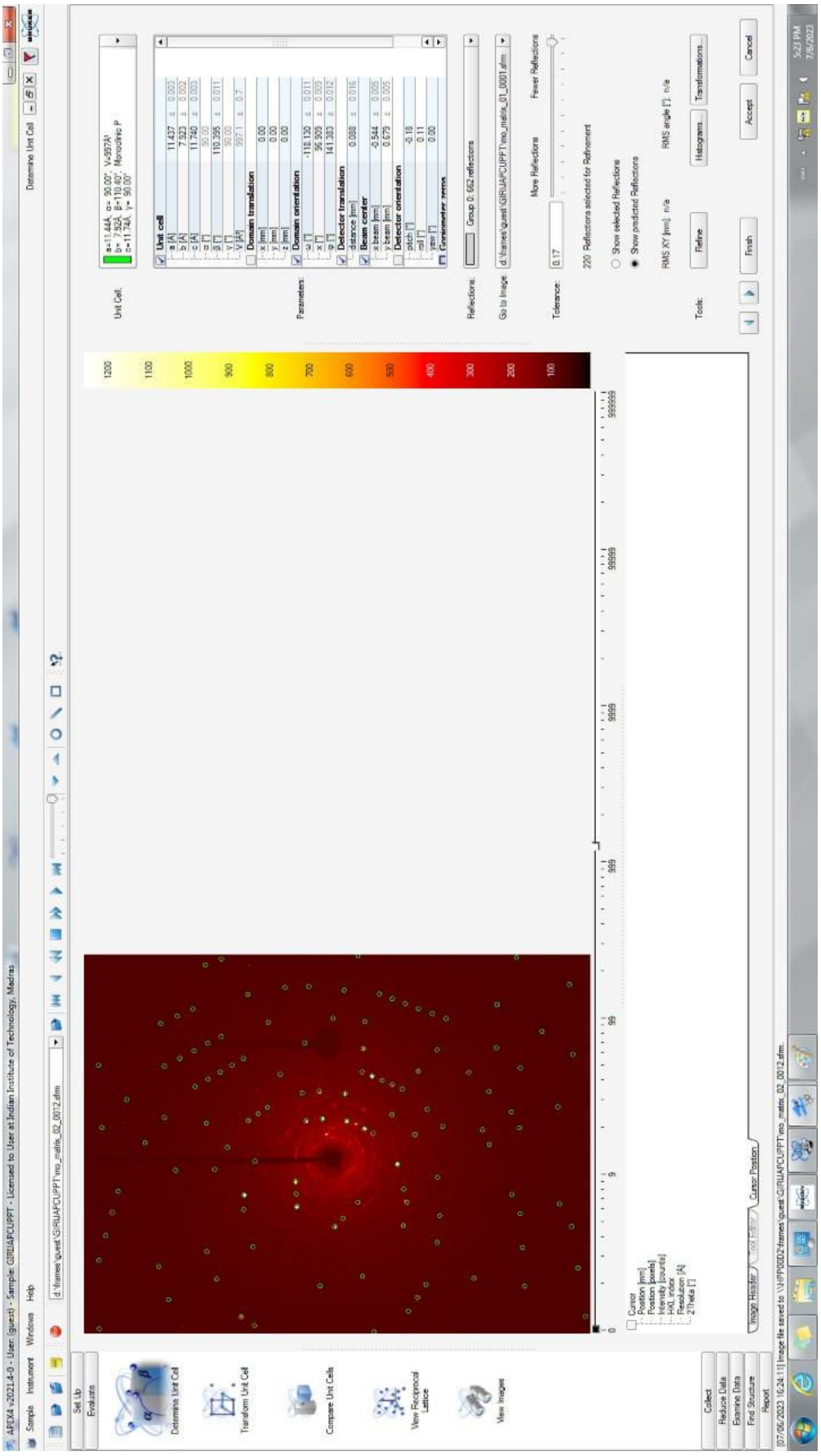

Figure 3. Single crystal XRD values of precipitate.

In TG curve, the weight loss is exhibited around 138 and 280ºC. The clear and distinct endothermic peak observed in the DTA curves indicates the excellent crystalline nature of the material. The material's stability for applications in laser technology is evident from its lack of decomposition up to the melting point, highlighting its capability to endure high temperatures. Sharp endotherm is an indication of solid-state transition for relatively pure material.

SINGLE CRYSTAL X-RAY DIFFRACTION ANALYSIS (FIGURE 3)

A Bruker AXS (Kappa APEX II) X-ray diffractometer was used to perform single crystal X-ray diffraction investigations. The lattice parameters of pyridine copper sulfate precipitate was determined as; a = 11.44 Å, b = 7.92 Å and c = 11.74 Å, $\alpha = 90^{o}$, $\beta = 110.40^{o}$ and $\gamma = 90^{o}$ and cell volume equal to 997 $Å^3$ for the green precipitate with monoclinic system in nature. The cell parameter values for pyridine copper sulfate precipitate there is a slight difference than pyridine values, whose cell parameter values are tabulated in the Table 1.

The slight difference in the cell parameter values and differing angles could be due to the formation of green precipitate by doping of copper metal to pyridine. Also, copper has made a difference in structure such that the structure of synthesized compound that has to be determined through data collection and refinement since it is a new attractive green precipitate material (Table 1).

Scanning Electron Microscopy with Energy Dispersive X-Ray Spectroscopy

The surface nature and appropriateness for device fabrication are discussed in the SEM study (JEOL JSM 5610lv), which is also used to check for flaws. There have been reports on the usefulness of various contaminants in altering the surface morphology. Figure 4(a–d) shows the surface morphology of pyridine copper sulfate precipitate, which shows the larger scatter center morphology with long voids and deep crack development on the surface of the material for different magnifications like 250, 500, 5000 and 10,000. Not only that, in higher magnification like 5000 and 10,000 the surface looked like cauliflower appearance. Table 2 gives the detailed atomic and mass percentage of different components present and the doped impurities actual percentage in pyridine copper sulfate precipitate inferred from EDS graph.

Table 1. Cell parameters values of pyridine copper sulfate precipitate.

Crystals	a (Å)	B (Å)	c (Å)	V (Å^3)	System
Pyridine copper sulfate precipitate	11.44	7.92	11.74	997	Monoclinic

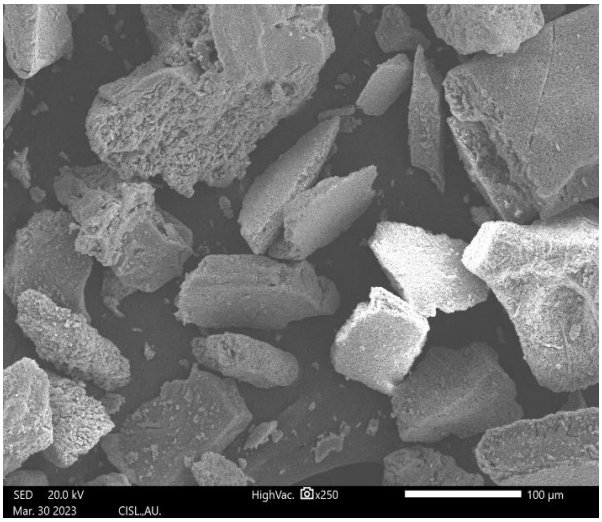

(a) Magnification 250

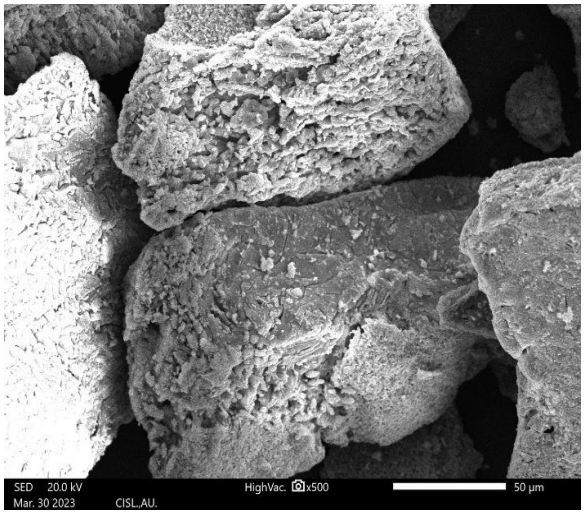

(b) Magnification 500

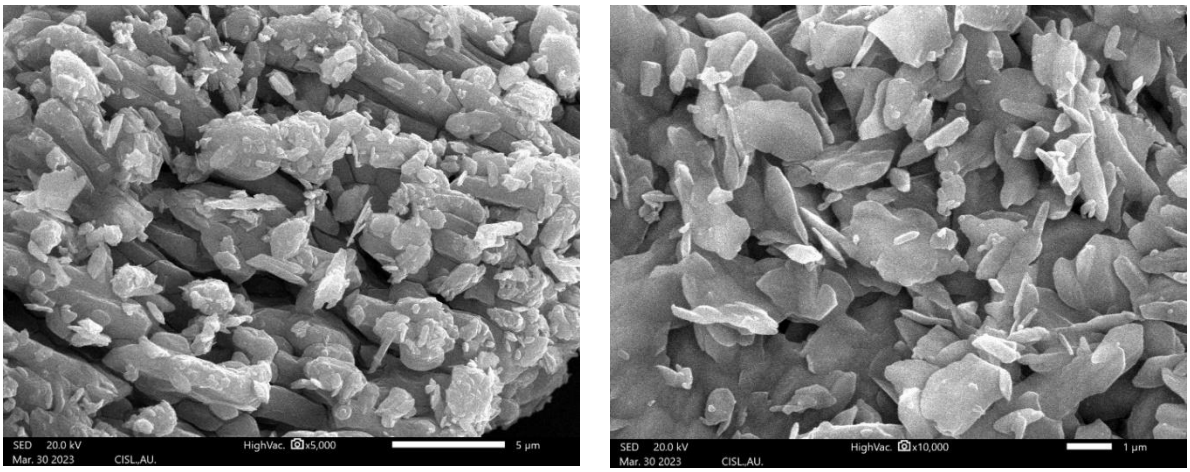

(C) Magnification 5000 (d) Magnification 10,000

Figure 4. Scanning electron micrographs of pyridine copper sulfate precipitate.

Table 2. Mass and atomic percentage of pyridine copper sulfate precipitate.

Element	Line	Mass%	Atom%
C	K	7.52 ± 0.10	14.06 ± 0.19
N	K	1.21 ± 0.06	1.94 ± 0.10
O	K	44.70 ± 0.21	62.77 ± 0.29
Mg	K	0.05 ± 0.02	0.04 ± 0.02
S	K	13.47 ± 0.09	9.44 ± 0.06
Cl	K	0.20 ± 0.02	0.13 ± 0.01
K	K	0.07 ± 0.02	0.04 ± 0.01
Cu	K	32.71 ± 0.28	11.56 ± 0.10
Zn	K	0.08 ± 0.05	0.03 ± 0.02
Total		100.00	100.00
Spc_004 fitting ratio 0.0303			

EDS graph confirms the presence of copper, sulfur, oxygen and so on (Figure 5). Surface analysis at various locations reveals that a significant amount of dopant copper has been integrated onto pyridine, causing it to be uneven throughout the surface and linked to an adsorption mechanism. Here doped copper is at the intensities of 500, 1500 , 4800 and 6700 counts to energy 0.8, 1, 8 and 8. 9 KeV where as other metals like zinc and magnesium and components like oxygen, nitrogen, sulfur, chlorine, and carbon are present as traces due to impurities present in the instrument. From Table 2 it is clear that copper's mass % is 32.71 and atom % 11.56.

Powder X-Ray Diffraction Analysis

Graphite monochromate CuKα radiation was used for the powder XRD examination. Doping does not lead to the emergence of new phases; however, there is a variation in the intensity of certain distinctive peaks. The XRD pattern of pyridine copper sulfate precipitate is given in Figure 6. We can notice some changes in the intensity of the diffraction pattern. The peak intensities are increased in the case pyridine copper sulfate XRD pattern which could be due to the higher incorporation of copper in the interstitial position. The XRD patterns of the specimen shows the multiple peaks with higher intensities ranging from 210 to 1670 as maximum peaks. The good crystallinity of the material is shown by Bragg's peaks at specific 2 angles 33° and 36° due to their sharpness and higher doping capacity of copper to nitrogen of pyridine through co-ordination bonding. The particle size can be calculated by Scherrer equation as follows:

$$T = K\lambda/(\beta \cos\theta).$$

where

t is the average crystallite size. λ is the X-ray wavelength, θ is the peak location in radians, and β is the integral breadth of reflection (in radians 2θ) is at 2θ. K is the Scherrer constant. The granularity of copper in the doped specimen is calculated as 7 nm.

Fourier Transform Infrared Spectroscopy

Pyridine copper sulfate precipitate FTIR spectra were acquired using the AVATAR 330 FT-IR instrument via the KBr pellet technique within the 600 to 4000 cm^{-1} range. The characteristic vibrational frequencies of pyridine copper precipitate are shown in Figure 7. There are some vibrational changes which are tabulated in Table 3. In Table 3, the higher short sharp peak at wavenumber 3585, 3495 cm^{-1} is assigned to O-H stretching vibration and a broad band in the range 3100–3590 cm^{-1} may be assigned due to N-H stretching vibration, a sharp peak at 1590 cm^{-1} is assigned to C=C-H in the aromatic ring, the sharp peak (vibrational frequency) at 1410 cm^{-1} is assigned to C=N of the aromatic ring of pyridine, wave number at 1110 cm^{-1} is assigned to C-N bond which is very sharp and intense, the lower wave number like 910 cm^{-1} is assigned to N-M that is the doped metal copper to nitrogen in pyridine ring to form a complex which could be confirmed from the structure refinement and data collection of the synthesized green pyridine copper sulfate precipitate and sharp peaks at 800 and 710 cm^{-1} are assigned to C-H out of plane aromatic bond.

UV-VISIBLE–NIR SPECTROSCOPY

UV-visible absorption and reflectance spectrum of pyridine copper sulfate precipitate in the range 200 to 2500 nm is shown in Figure 8a and b. The higher transmittance in the visible region could lead to the application of this formed precipitate in the optical windows. In absorbance spectrum the absorption is maximum at 2313 nm and 2387 nm whereas minimum at 285 and 847 nm indicating the synthesized material is possessing higher optical quality. In the reflectance spectrum, the doping of copper drastically increases the reflectance at 580 nm (lowering of absorbance) and hence we can conclude that copper is a useful dopant. The band gap energy for the synthesized green precipitate is calculated by using the formulae $E_g = h\ c\ /\ \lambda_{max}$ as 4.36 eV for absorbance at lower cutoff wavelength and 2.14 eV for reflectance at higher cutoff wavelength inferring the higher the band gap energy the higher will be its optical property of the material using.

$$E_g = 1.243 \times 10^3 / \lambda_{max},$$

where

h = Planck's constant and

c = velocity of light

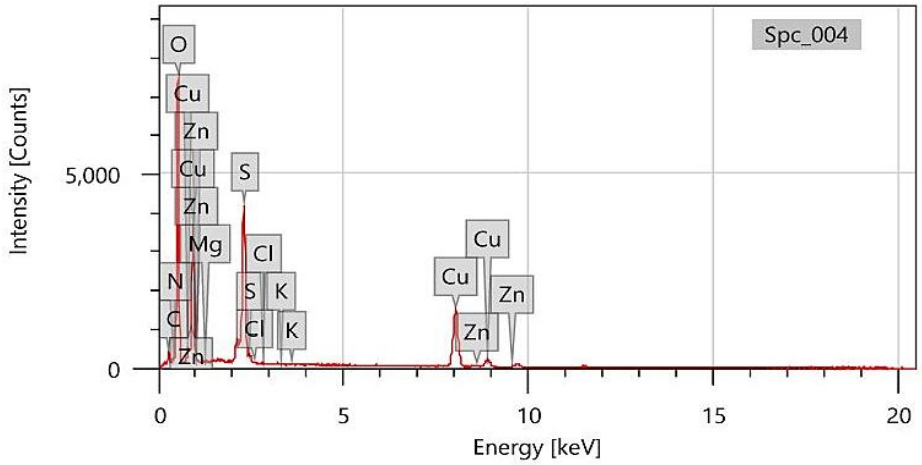

Figure 5. Energy-dispersive X-ray spectroscopy (EDS) graph of pyridine copper sulfate precipitate.

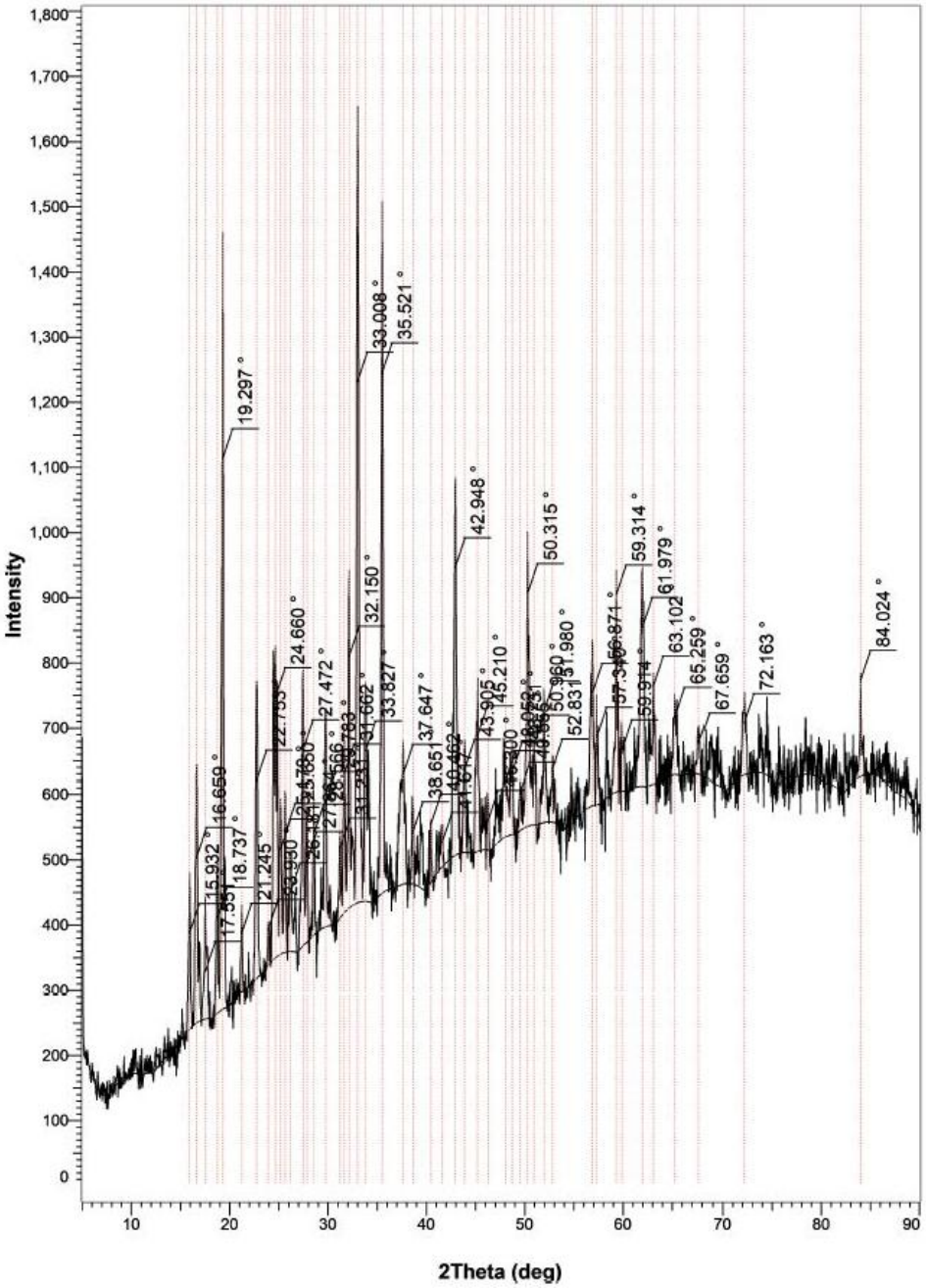

Figure 6. Powder X-ray diffraction (XRD) graph of pyridine copper sulfate precipitate.

Table 3. Vibrational frequencies of copper-doped pyridine precipitate.

S. No	Wavenumber of Copper-Doped Pyridine Sulfate Precipitate (cm^{-1})	Assignment
1.	3585, 3495	O-H
2.	3100–3590	N-H
3.	1590	C=C
4.	1410	C=N
5.	1110	C-N
6.	910	N-M
7.	800, 710	C-H (aromatic bond)

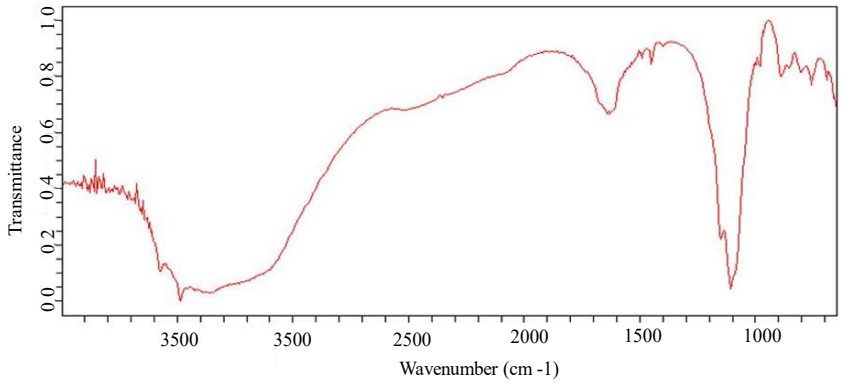

Figure7. Fourier transform infrared (FTIR) spectra of pyridine copper sulfate crystal.

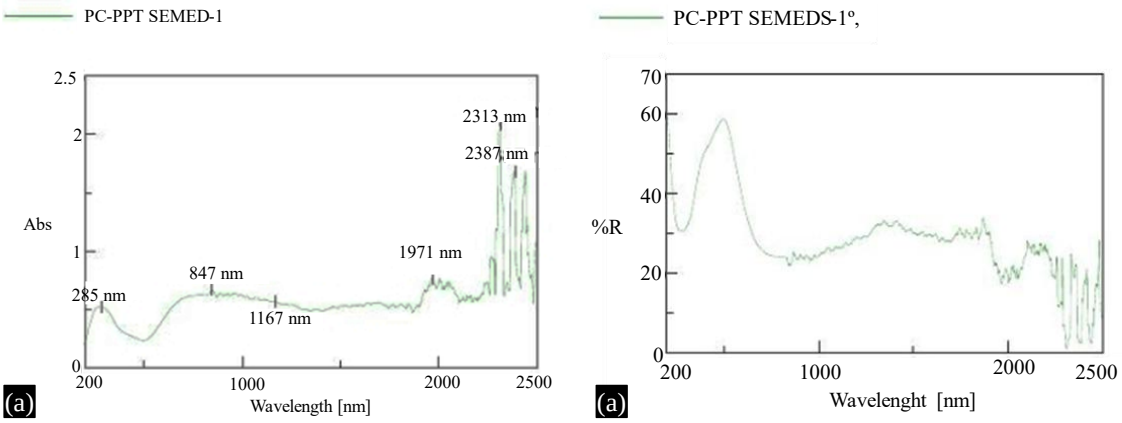

Figure 8. (a) Absorbance of pyridine copper sulfate precipitate. (b) Reflectance of pyridine copper sulfate precipitate.

CONCLUSION

Pyridine containing drugs are used as antimicrobial, antiviral, anticancer, antioxidant, antimalarial, antihypertensive, antidiabetic, antiamebic, psychopharmacological, antagonists and anti-inflammatory agents. The slow evaporation solution growth approach was used to produce pyridine copper sulfate precipitate with a crystalline quality that is comparatively good. The XRD, FTIR, SEM-EDS, UV-visible-NIR spectroscopy growth techniques have been used to study the influence of copper doping on pyridine. Incorporation of copper on pyridine and the percentage of doped amount is well studied by EDS and the surface morphology of the so-formed pyridine copper sulfate precipitate. The powder XRD and FTIR studies reveals that the doping of copper causes a small change in intensity and vibrational patterns, respectively. Structural studies indicate that the crystal is under stress and the size of dopant in granularity is observed as a result of doping. Single crystal XRD reveals that the synthesized crystal is with Monoclinic system with differing angles inferring that the so-formed precipitate (material) is a new compound and its structure should be refined. Optical studies reveal that the synthesized material could be applied to the optical windows and laser technology.

REFERENCES

1. Saravanan N, Ravisankar V, Chithambaram V. Growth and characterization of novel semi organic nonlinear optical urea lead acetate single crystal by solution growth technique. J Mater Sci Mater Electron. 2018; 29: 5009–5013.
2. Shah SH, Bristowe PD. First-principles density functional study of polarization–strain coupling in bismuth titanate. J Phys Condens Matter. 2010; 22 (38): 385902.
3. Oliver SA, Yoon SD, Kozulin I, Chen ML, Vittoria C. Growth and characterization of thick oriented barium hexaferrite films on MgO (111) substrates. Appl Phys Lett. 2000; 76 (24): 3612–3614.

4. Prasad LG, Krishnakumar V, Nagalakshmi R. Growth and characterization of semi-organic nonlinear optical crystal: sodium 2,4-dinitrophenolate monohydrate. Spectrochim Acta Part A Mol Biomol Spectrosc. 2013; 110: 377–382.
5. Hanumantharao R, Kalainathan S. Growth, spectroscopic, dielectric and nonlinear optical studies of semi organic nonlinear optical crystal–l-alanine lithium chloride. Spectrochim Acta Part A Mol Biomol Spectrosc. 2012; 86: 80–84.
6. Rani N, Vijayan N, Maurya KK, Haranath D, Saini P, Rathi B, Wahab MA, Bhagavanarayana G. Studies on the effect of polymer coating on solution grown hygroscopic non-linear optical single crystal of L-lysine monohydrochloride. Spectrochim Acta Part A Mol Biomol Spectrosc. 2012; 97: 871–875.
7. Bouchouit K, Bendeif EE, Ouazzani HE, Dahaoui S, Lecomte C, Benali-Cherif N, Sahraoui B. Correlation between structural studies and third order NLO properties of selected new quinolinium semi-organic compounds. Chem Phys. 2010; 375 (1): 1–7.
8. Akselrod MS, Bruni FJ. Modern trends in crystal growth and new applications of sapphire. J Cryst Growth. 2012; 360: 134–145.
9. Bouchouit K, Essaidi Z, Abed S, Migalska-Zalas A, Derkowska B, Benali-Cherif N, Mihaly M, Meghea A, Sahraoui B. Experimental and theoretical studies of NLO properties of organic–inorganic materials base on p-nitroaniline. Chem Phys Lett. 2008; 455 (4–6): 270–274.
10. Vivek P, Suvitha A, Murugakoothan P. Growth, spectral, anisotropic, second and third order nonlinear optical studies on potential nonlinear optical crystal anilinium perchlorate (AP) for NLO device fabrications. Spectrochim Acta Part A Mol Biomol Spectrosc. 2015; 134: 517–525.
11. Akdas-Kilig H, Malval JP, Morlet-Savary F, Singh A, Toupet L, Ledoux-Rak I, Zyss J, Le Bozec H. The synthesis of tetrahedral bipyridyl metallo-octupoles with large second-and third-order nonlinear optical properties. Dyes Pigments. 2012; 92 (1): 681–688.
12. Srineevasan R, Rajasekaran R. Growth and optical studies of 2-aminopyridine bis thiourea zinc sulphate (2-APTZS) single crystals for NLO applications. J Mol Struct. 2013; 1048: 238–243.
13. Gowri S, Devi TU, Sajan D, Bheeter SR, Lawrence N. Spectral, thermal and optical properties of adenosinium picrate: a nonlinear optical single crystal. Spectrochim Acta Part A Mol Biomol Spectrosc. 2012; 89: 119–122.
14. Kumar P, Gupta R. The wonderful world of pyridine-2,6-dicarboxamide based scaffolds. Dalton Trans. 2016; 45 (47): 18769–18783.
15. M ü ller S, Sanders DA, Di Antonio M, Matsis S, Riou JF, Rodriguez R, Balasubramanian S . Pyridostatin analogues promote telomere dysfunction and long-term growth inhibition in human cancer cells. Org Biomol Chem. 2012; 10 (32): 6537–6546.
16. Li J, Tilbury CJ, Kim SH, Doherty MF. A design aid for crystal growth engineering. Prog Mater Sci. 2016; 82: 1–38.
17. Wood JS, Keijzers CP, De Boer E. The ESR spectra of the pure and zinc doped hexakis pyridine-N-oxide cuprate ion. Chem Phys Lett. 1977; 51: 489–492.
18. Usman MU, Faruque MO. Applications of synchrophasor technologies in power systems. Journal of Modern Power Systems and Clean Energy. 2019; 7(2): 211–26.

